Dyes and Pigments 173 (2020) 107927

Contents lists available at ScienceDirect

Dyes and Pigments

journal homepage: http://www.elsevier.com/locate/dyepig

Effect of interface modification in polymer solar cells: An in-depth investigation of the structural variation of organic dye for interlayer material

Mijin Jeong [a], Ho Cheol Jin [a], Jun Ho Lee [a], Doo Kyung Moon [b], Joo Hyun Kim [a,*]

[a] Department of Polymer Engineering, Pukyong National University, Busan, 48513, South Korea
[b] Division of Chemical Engineering, Konkuk University, Seoul, 05029, South Korea

ARTICLE INFO

Keywords:
Small-molecule dye
Dipole moment
Alkyl chain length
Polymer solar cell

ABSTRACT

In order to investigate the effect of the structural variation of interlayer materials on the photovoltaic properties of polymer solar cells (PSCs) in depth, we designed and synthesized three types of small-molecule dyes with a structure of 1,1′-bis(1-alkyl)-4,4′-bipyridine-1,1′-diium benzenesulfonate (**V-alkyl-OTs**). Here, the alkyl groups were butyl, hexyl, and dodecyl, which denoted as **C4**, **C6**, and **C12**, respectively. The magnitudes dipole moments will be in the order of **V–C4-OTs** < **V–C6-OTs** < **V–C12-OTs** due to the increased the alkyl chain length from **C4** to **C12**. The work function of the ZnO layer with **V-alkyl-OTs** is exhibited to depend on the alkyl chain length, indicating that a Schottky barrier can be tuned by the size of cation part. Thus, The power conversion efficiencies (PCEs) of the PSCs based on the blend of PTB7 and $PC_{71}BM$ as the photoactive layer with **V-alkyl-OTs** were improved over for the device with pristine ZnO (without **V-Alkyl-OTs**) from 7.6% (short circuit current (J_{sc}) = 16.0 mA/cm^2, open circuit voltage (V_{oc}) = 0.72 V, fill factor (FF) = 65.6%) to 8.1% (**V–C4-OTs**, J_{sc} = 16.8 mA/cm^2, V_{oc} = 0.73 V, FF = 65.9%), 8.3% (**V–C6-OTs**, J_{sc} = 17.2 mA/cm^2, V_{oc} = 0.72 V, FF = 67.3%), and 8.6% (**V–C12-OTs**, J_{sc} = 18.0 mA/cm^2, V_{oc} = 0.72 V, FF = 66.4%). The enhancement of the PCE is strongly related to the alkyl chain length, and the major contribution was by the improvement of the J_{sc} due to the reduction in the energy offset at the cathode interface.

1. Introduction

Polymer solar cells (PSCs) increase affordability because the PSCs can be fabricated by the solution process [1–4]. Previously, the power conversion efficiency (PCE) of PSCs has been reached 15% [5,6] by the development of efficient photoactive materials [6–17] or through device engineering [18–47].

For PSC device engineering, the charge collection from the photoactive layer to the electrodes is an important parameter for efficient devices. Therefore, adjusting the energy offset at the electrode interface is a principal issue to be considered. The zinc oxide (ZnO) layer, which has been widely used as the cathode buffer layer (CBL), has been modified to optimize the charge collection ability by inserting conjugated/non-conjugated polymer electrolytes [18–31], small-molecular electrolytes [32–38], or other materials [39–47].

For electron collection, we have reported the synthesis and application of various non-conjugated/conjugated electrolytes for the CBL of PSCs. We have also reported on the effects of anion size [18,22] or hydroxyl group [32] of the organic electrolytes on the photovoltaic properties. In addition, the alkyl chain-length effect of using viologen-based polymer dyes as the electron transporting layer was investigated in conventional PSCs [18]. The results suggest that longer alkyl chains are more effective than shorter chains for the fabrication of efficient PSCs. Viologen derivatives are well known as electrochromic dyes [18,22,29,48], which show very high electron affinity, high-lying reduction potential, and good solubility in water or alcoholic aqueous solvent. Thus, viologen derivatives can be applied to the CBL for PSCs.

Based on our previous studies, as shown in Fig. 1 **(a)**, we designed and synthesized three types of small-molecule dyes with a structure of 1,1′-bis(1-alkyl)-4,4′-bipyridine-1,1′-diium benzenesulfonate (**V-alkyl-OTs**) to investigate the effects of the alkyl chain length on the photovoltaic properties. The alkyl groups examined butyl, hexyl, and dodecyl, denoted as **C4**, **C6**, and **C12**, respectively. The magnitudes of the dipole moment of ionic compounds are proportional to the size of the

* Corresponding author.
E-mail address: jkim@oknu.ac.kr (J.H. Kim).

https://doi.org/10.1016/j.dyepig.2019.107927
Received 7 August 2019; Received in revised form 17 September 2019; Accepted 23 September 2019
Available online 25 September 2019

compounds. Thus, the magnitudes of the dipole moments of **V-alkyl-OTs** structures will be in the order of **C4** < **C6** < **C12**. A longer alkyl chain can induce a larger dipole moment, even when the alkyl group is attached to the amino cation, there is a similar correlation between the alkyl chain length and the dipole moment [49–52]. Therefore, a larger dipole moment of **V-alkyl-OTs** further will reduce the energy offset at the electrode interface, especially between the electron transporting layer (ZnO) and the photoactive layer. However, an excessively long alkyl chain would reduce the PCE by enhancing the insulating property of the layer. Thus, it is important to find out appropriate length of alkyl chain in a trade-off relationship between the dipole moment and electrical property of materials. Following this basic concept, we selected butyl (**C4**), hexyl (**C6**), and dodecyl (**C12**) as the alkyl groups and fabricated the PSCs with **V-alkyl-OTs** as the CBL. As illustrated in Fig. 2 (b), the devices were fabricated with a configuration of ITO/ZnO/-**V-alkyl-OTs**/PTB7:$PC_{71}BM$/MoO_3/Ag. The PCEs of the device with ZnO/**V-alkyl-OTs** were improved from 7.6% (short circuit current (J_{sc}) = 16.0 mA/cm^2, open circuit voltage (V_{oc}) = 0.72 V, fill factor (FF) = 65.6%) with pristine ZnO to 8.1% (**C4**, J_{sc} = 16.8 mA/cm^2, V_{oc} = 0.73 V, FF = 65.9%), 8.3% (**C6**, J_{sc} = 17.2 mA/cm^2, V_{oc} = 0.72 V, FF = 67.3%), and 8.6% (**C12**, J_{sc} = 18.0 mA/cm^2, V_{oc} = 0.72 V, FF = 66.4%). The enhancement of the PCE is strongly related to alkyl chain length, contributed mostly by the improvement of the J_{sc} due to the reduction in the energy offset at the cathode interface.

2. Results and discussions

2.1. Characterization of V-alkyl-OTs and V-alkyl-OTs coated ZnO surface

As described in the supporting information, **V-alkyl-OTs** were successfully synthesized. The chemical structures of the synthesized compounds were well characterized by the ^{1}H and ^{13}C NMR spectroscopy and elemental analysis. The ^{1}H NMR, ^{13}C NMR, MASS spectra of **V-alkyl-OTs** are showed in Figs. S1 and S2. Thermogravimetric analysis (TGA) (Fig. S3) of **V-alkyl-OTs** was performed with a heating rate of 10 °C/min under the air atmosphere to investigate thermal stability of compounds. The **V-alkyl-OTs** with **C4**, **C6**, and **C12** were thermally stable (no more than 5% loss in mass) up to 300, 294, and 296 °C, respectively.

To analyze the existence of **V-alkyl-OTs** on the surface of ZnO, we performed X-ray photoelectron spectroscopy (XPS) on the compounds. Fig. 2 shows the XPS spectra of ZnO with and without **V-alkyl-OTs**. Signals at 400 and 167 eV correspond to N 1s and S 2p, respectively. Peaks at 1044 and 1021 eV in the XPS spectrum of ZnO correspond to Zn 2p1/2 and 2p3/2, respectively. The peaks in XPS spectra of ZnO with **V-alkyl-OTs** shifted toward higher energy because the Zn atoms become more electron-rich than in the ZnO without **V-alkyl-OTs**.

The atomic force microscopy (AFM) images were observed of the **V-alkyl-OTs**-treated ZnO layer (Fig. S4). The surface morphology of ZnO treated with **V-alkyl-OTs** was observed to be similar to the pristine ZnO. The average surface roughness (R_a) of **V-alkyl-OTs** with **C4**, **C6**, and **C12** measurements were 1.33, 1.37, and 1.47 nm, respectively. The R_a gradually increased with the length of the alkyl chain. The water contact angle analysis (Fig. S5) was performed to investigate surface properties. Interestingly, the water contact angle of the **V-alkyl-OTs** coated ZnO layer gradually increased with increase in the alkyl chain length, 18.8° for **C4**, 21.1° for **C6**, and 21.6° for **C12**, which were smaller than the angle of pristine for the pristine ZnO surface (28.6°). The Photoluminescence (PL) spectra (Fig. S6) of ZnO and **V-alkyl-OTs** treated-ZnO were measured to observe the defect coverage of the ZnO surface. However, there was no discernible change in the PL spectra of **V-alkyl-OTs** treated-ZnO layer.

2.2. Photovoltaic properties

To demonstrate the effect of **V-alkyl-OTs** on the performance of the device, **V-alkyl-OTs** was used as the CBL in PSCs with the device configuration of ITO/**V-alkyl-OTs**/ZnO/PTB7:$PC_{71}BM$/MoO_3/Ag (shown in Fig. 1 **(b)**). The typical thickness of the **V-alkyl-OTs** layer was ~5 nm. Fig. 3 shows current the density-voltage curves of PSCs with the **V-alkyl-OTs** layer as the CBL under illumination. The photovoltaic

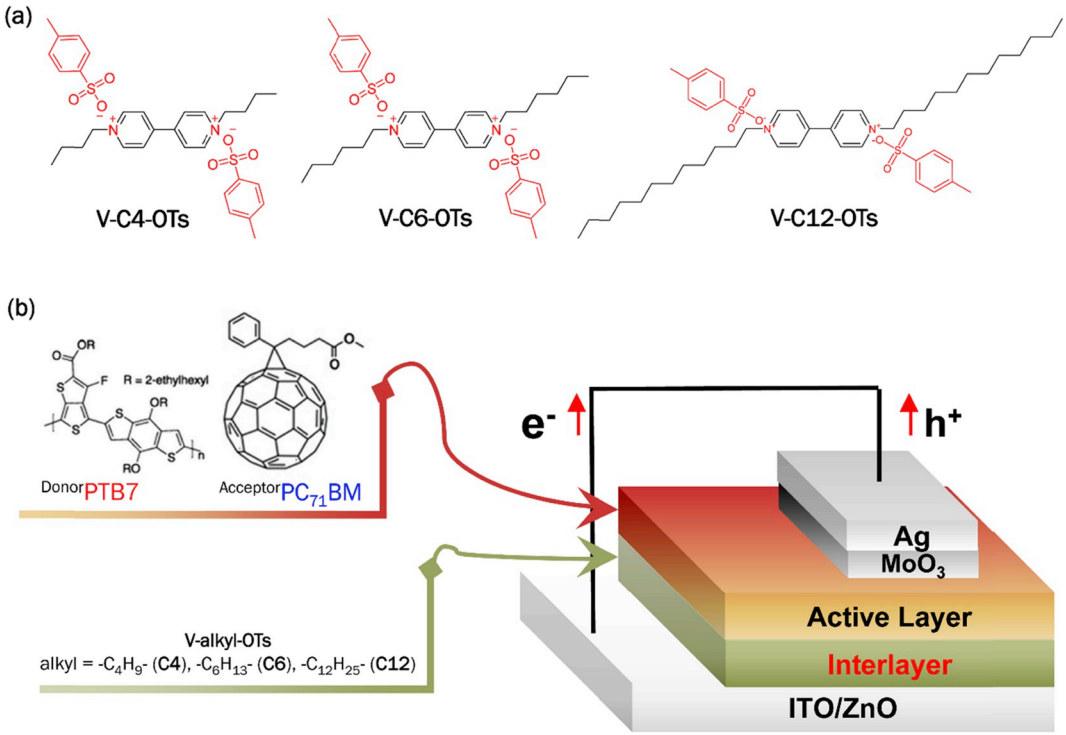

Fig. 1. (a) The chemical structures of V-alkyl-OTs (b) the device structure in this research.

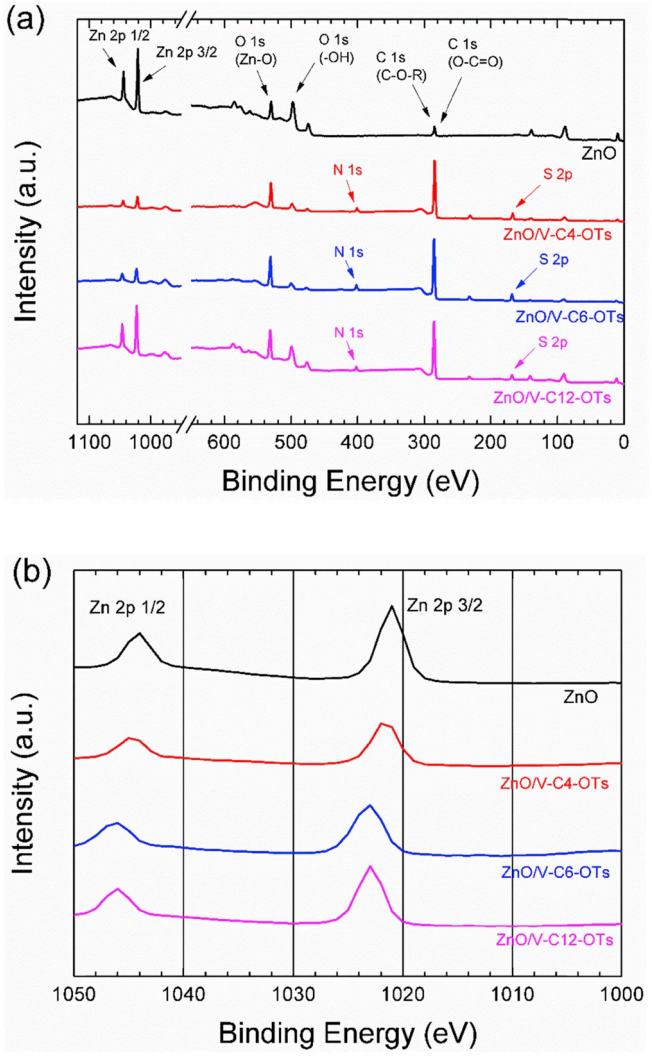

Fig. 2. (a) XPS survey spectra and (b) Zn 2p spectra of ZnO with and without **V-alkyl-OTs**.

parameters are summarized in Table 1. As shown in Fig. 3 and Table 1, a noticeable correlation was found between the alkyl chain length of **V-alkyl-OTs** and the PCE of the device. The PCE of the devices with **V-alkyl-OTs** layer was improved with the increase in the alkyl chain length. The PCEs exhibited 8.1% (**C4**, $J_{sc} = 16.8\ mA/cm^2$, $V_{oc} = 0.73\ V$, FF = 65.9%), 8.3% (**C6**, $J_{sc} = 17.2\ mA/cm^2$, $V_{oc} = 0.72\ V$, FF = 67.3%), and 8.6% (**C12**, $J_{sc} = 18.0\ mA/cm^2$, $V_{oc} = 0.72\ V$, FF = 66.4%), which are greater than the results for the device with untreated-ZnO layer. (PCE = 7.6%, $J_{sc} = 16.0\ mA/cm^2$, $V_{oc} = 0.72\ V$, FF = 65.6%). Thus, a significant enhancement of 13.2% was observed in the device with the **V–C12-OTs** layer compared to the device with the untreated ZnO layer. The enhancement of J_{sc} was the main contribution to the PCE improvement.

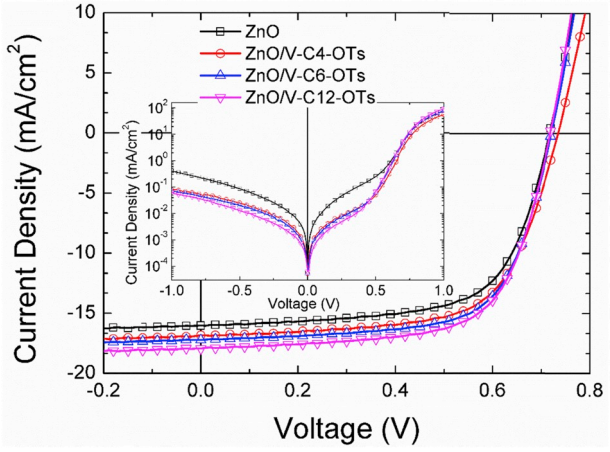

Fig. 3. Current density–voltage curves of PSCs ZnO, ZnO/**V-alkyl-OTs** under illumination (inset: in the dark condition) in this research.

We performed the Kelvin probe microcopy (KPM) measurements to investigate the effect of **V-alkyl-OTs** on the J_{sc}. As mentioned before, the reduction of the energy offset at the interface is a crucial factor for a high J_{sc} because a large energy offset interrupts the charge collection [17–20, 23,35]. Fig. 4 shows the energy diagram with the effective work function of the ZnO layer with and without **V-alkyl-OTs**. As shown in Fig. 4 **(a)**, the energy offset (ΔE) of the **V-alkyl-OTs** treated-ZnO surface exhibits 0.37 (**C4**), 0.30 (**C6**), and 0.23 (**C12**) eV, where the ΔE is defined as the difference between the LUMO of $PC_{71}BM$ and the effective work function on the treated-ZnO surface. The values were smaller than that of ZnO surface (0.44 eV) and the trend of ΔE is highly correlated to the length of the alkyl chain. The calculated J_{sc} from the IPCE spectra (Fig. S7) also corresponded with the J_{sc} of the PSCs under the 1.5 G condition.

To investigate the effect of **V-alkyl-OTs** on the electron collection capability, the electron-only devices with configurations of ITO/ZnO (25 nm) with and without **V-alkyl-OTs**/$PC_{71}BM$ (60 nm)/Al (100 nm) were fabricated and tested (Fig. 5). These devices exhibit a space charge limited current (SCLC) behavior above the built-in voltage, which is represented by the Mott-Gurney equation [53].

$$J = \frac{9}{8}\varepsilon_0\varepsilon_r\mu\frac{E^2}{L}$$

where J is the current density, μ is the charge mobility, E is the electric field, $\varepsilon_0\varepsilon_r$ is the permittivity of the active layer, and L is the thickness of the ZnO layer. Using $\varepsilon_r = 3.9$ for $PC_{71}BM$ to calculate the electron mobility. The electron mobility of the devices with **V-alkyl-OTs** were 2.43×10^{-3} (**C4**), 2.49×10^{-3} (**C6**), 2.89×10^{-3} (**C12**) $cm^2V^{-1}s^{-1}$, which are slightly higher values than the measured electron mobility of the ZnO layer without **V-alkyl-OTs** ($2.24 \times 10^{-3}\ cm^2V^{-1}s^{-1}$). The trend of electron mobility data appeared to be correlated to the alkyl chain length of **V-alkyl-OTs**, but the change in electron mobility with **V-alkyl-OTs** is not significantly different from the value for the pristine ZnO. Similar features were found in the series resistance (R_s) data (Table 1). The R_s data of the devices with **V-alkyl-OTs** were almost similar to for the device based on pristine ZnO. However, the turn-on voltages of the devices with **V-alkyl-OTs** were 1.02 (**C4**), 0.91 (**C6**), and 0.73 V (**C12**), which are smaller than that of the device without **V-alkyl-OTs** (1.39 V). The turn-on voltage [54] is strongly correlated with the electron collection capability at the interface. The results agree with the increase in the J_{sc} and the decrease in the energy offset at the interface.

Electronic impedance spectroscopy (EIS) was performed to investigate the carrier transport and recombination mechanism. The EIS spectra (Fig. 6) were linearly fitted to estimate the recombination resistance (R_{rec}). The larger EIS semi-circle reflects a greater recombination resistance. The higher R_{rec} values are related to the extraction of the charge at the ZnO interfaces. The R_{rec} of the devices with **V-alkyl-OTs** were 1360 (**C4**), 1650 (**C6**), 1950 (**C12**) kΩ, which are higher than the R_{rec} of the device with pristine ZnO (1230 kΩ). The results are consistent with the PCEs of the device.

In order to further understand the effect of **V-alkyl-OTs** on the charge transporting and collection properties, we plotted and analyzed the photocurrent density ($J_{ph} = J_L - J_D$) as a function of the effective voltage ($V_{eff} = V_0 - V_{app}$), where J_L is the current density under illumination, J_D is the current density under dark conditions, V_0 is the voltage at which $J_{ph} = 0$ and V_{app} is the applied voltage, respectively. The

Table 1
The performances of PSCs with ZnO layer showing the best PCE. The averages and deviations (20 devices are averaged) are summarized in parentheses.

Buffer Layer	J_{sc} (mA/cm^2)	V_{oc} (V)	*FF* (%)	*PCE* (%)	R_s (Ω cm^2)	[a]Calculated J_{sc} (mA/cm^2)
ZnO	16.0 (15.9 ± 0.2)	0.72 (0.72 ± 0.00)	65.6 (65.4 ± 0.35)	7.6 (7.5 ± 0.1)	2.9	15.9
V–C4-OTs treated-ZnO	16.8 (16.8 ± 0.1)	0.73 (0.73 ± 0.00)	65.9 (65.8 ± 0.14)	8.1 (8.1 ± 0.1)	2.9	17.0
V–C6-OTs treated-ZnO	17.2 (17.2 ± 0.1)	0.72 (0.72 ± 0.00)	67.3 (66.7 ± 1.22)	8.3 (8.2 ± 0.1)	2.6	17.4
V–C12-OTs treated-ZnO	18.0 (17.7 ± 0.3)	0.72 (0.72 ± 0.00)	66.4 (66.0 ± 0.64)	8.6 (8.4 ± 0.2)	2.2	18.1

[a] Calculated from the IPCE spectra.

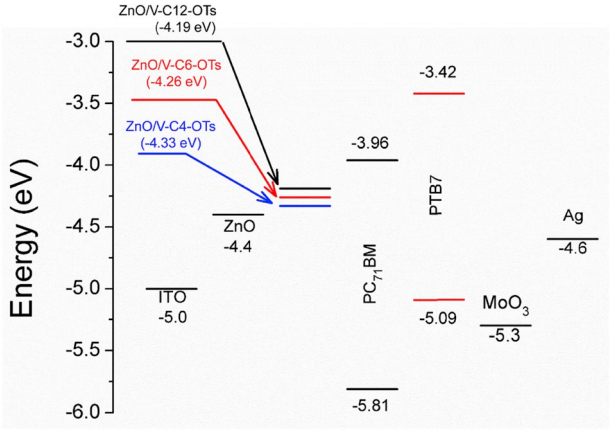

Fig. 4. The work function of **V-alkyl-OTs** treated-ZnO and the energy diagram of the device in this research.

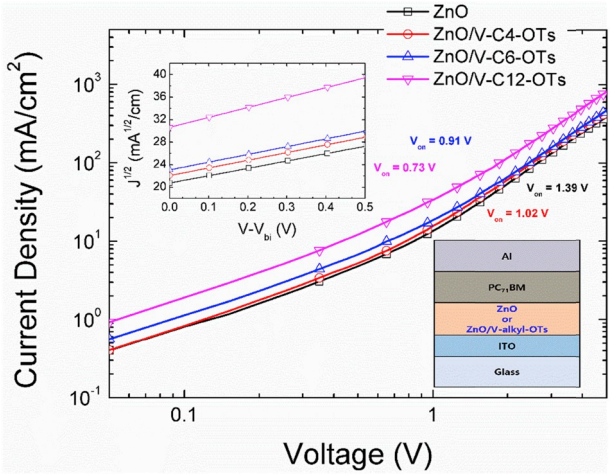

Fig. 5. Current density–voltage curves of electron-only device with a configuration of ITO/ZnO (25 nm) with or without **V-alkyl-OTs**/$PC_{71}BM$ (60 nm)/Al (100 nm). (inset: with fitted line, V: applied voltage, V_{bi}: built-in voltage, V_{on}: turn-on voltage).

voltages (V_{sat}) at which J_{ph} show the transition to the saturation regime were 0.275 V (ZnO), 0.199 V (ZnO/**V–C4-OTs**), 0.178 V (ZnO/**V–C6-OTs**), and 0.173 V (ZnO/**V–C12-OTs**) (shown in Fig. 7 **(a)**). Interestingly, the results strongly agree with the trend of the J_{sc} and the PCEs of the devices, because the small V_{sat} means the low energy barrier in the device. Using the carrier-transporting and collecting probability in the flat region of the J_{ph} from the ratio of J_{ph}/J_{sat} can be estimated, where the J_{sat} is the saturated current density and calculated from the convergence value of J_{ph}. (Fig. 7 **(b)**) The carrier transporting and collecting probabilities at the J_{sc} condition were 93.17% (ZnO), 93.61% (ZnO/**V–C4-OTs**), 94.00% (ZnO/**V–C6-OTs**), 94.21% (ZnO/**V–C12-OTs**), respectively. Finally, the maximum exciton generation rate ($G_{max} = J_{ph}/(q/L)$) at the V_{sat}, in which the q is the elementary charge

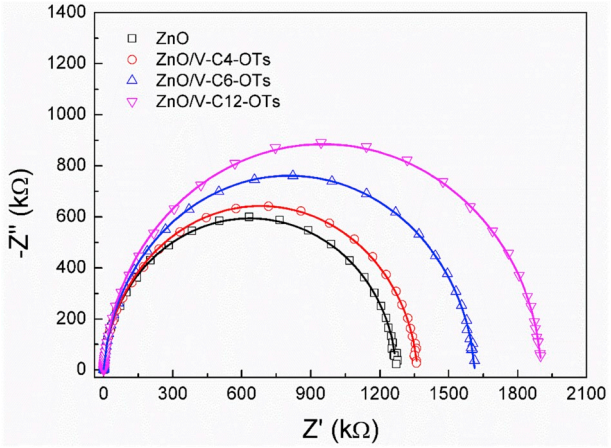

Fig. 6. Impedance spectra of the PSCs based on ZnO without and with **V-alkyl-OTs.**

and the L is the thickness of the active layer, was calculated as 1.141×10^{28} (ZnO), 1.254×10^{28} (ZnO/**V–C4-OTs**), 1.232×10^{28} (ZnO/**V–C6-OTs**), and 1.298×10^{28} (ZnO/**V–C12-OTs**) $m^{-3}s^{-1}$, respectively. No apparent changes were observed in G_{max}, because the G_{max} correlates with the absorbance of the active layer. As mentioned before, the tendency of V_{sat} and the carrier transporting and collecting probability agrees with the increase in J_{sc} and the decrease in the energy barrier. This correlation means that the devices with ZnO/**V-alkyl-OTs** exhibited a decreased charge recombination, and an increased charge collection capability at the cathode interface along the dipole moment of the applied materials.

3. Conclusion

A series of small-molecule dyes based on dialkyl viologen with different alkyl chain length have been synthesized and demonstrated as the CBL layer for PSCs to investigate the structural variation of interlayer materials. The PCEs of the device with **V-alkyl-OTs** as the CBL were 8.1 (**C4**), 8.3 (**C6**), and 8.6% (**C12**), respectively. These values are better than the PCE of the device with pristine ZnO (7.6%) due to the formation of the interface dipole at the cathode interface by the thin layer of **V-alkyl-OTs**. Also, we found that the PCEs of the PSCs depend on the alkyl chain length of interlayer materials because longer alkyl chain induces a larger interface dipole. Similarly, the work function of the ZnO layer with **V-alkyl-OTs** is exhibited to depend on the size of cation part, indicating that a Schottky barrier can be tuned by the size of cation part. The major significant contribution to the enhancement of the PCE was through the improvement of the J_{sc} due to the reduction of the energy offset at the cathode interface. From the results, a longer alkyl chain induces a larger interface dipole, and the enhancement of the PCE is strongly related to alkyl chain length.

Declaration of competing interest

There is no conflict of interest.

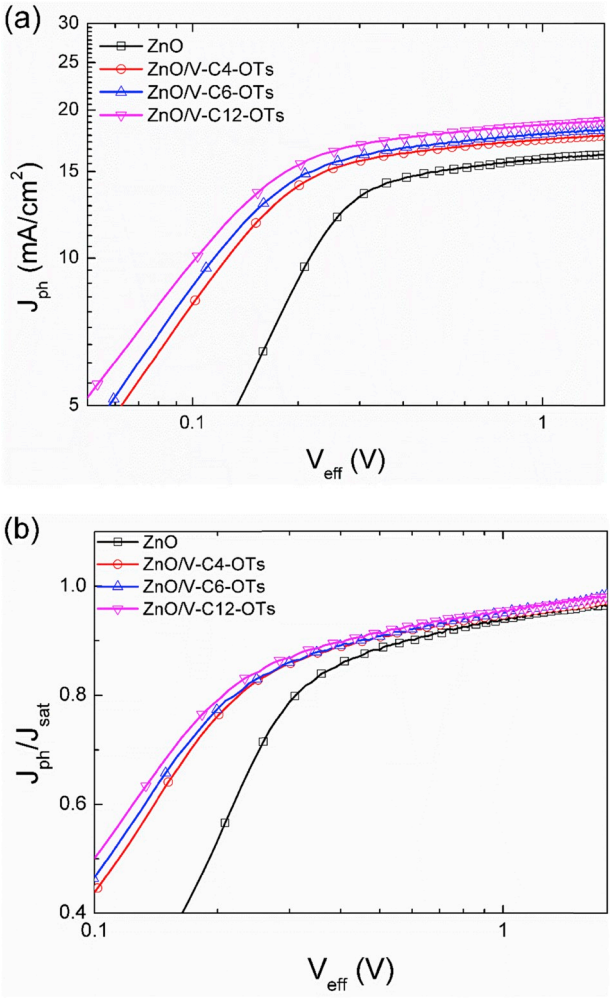

Fig. 7. (a) Photo-generated current density (J_{ph}) and (b) the carrier transporting and collecting probability vs. effective voltage (V_{eff}) plots of the PSCs.

Acknowledgments

This research work was supported by the New & Renewable Energy Core Technology Program of the Korea Institute of Energy Technology Evaluation and Planning (KETEP) granted financial resource from the Ministry of Trade, Industry & Energy, Republic of Korea (20153010140030, 2018201010636A) and was supported by Basic Science Research Program through the National Research Foundation of Korea (NRF) funded by the Ministry of Education (2019R1A2C1002585).

M. Jeong, H. C. Jin contributed equally to this work.

Appendix A. Supplementary data

Supplementary data to this article can be found online at https://doi.org/10.1016/j.dyepig.2019.107927.

References

[1] Yu G, Gao J, Hummelen JC, Wudl F, Heeger AJ. Polymer photovoltaic cells: enhanced efficiencies via a network of internal donor-acceptor heterojunctions. Science 1995;270:1789–91.
[2] Gunes S, Neugebauer H, Sariciftci NS. Conjugated polymer-based organic solar cells. Chem Rev 2007;107:1324–38.
[3] Lu L, Zheng T, Wu Q, Schneider AM, Zhao D, Yu L. Recent advances in bulk heterojunction polymer solar cells. Chem Rev 2015;115:12666–731.
[4] Su Y-W, Lan S-C, Wei K-H. Organic photovoltaics. Mater Today 2012;15:554–62.
[5] Yuan J, Zhang Y, Zhou L, Zhang G, Yip H-L, Lau T-K, Lu X, Zhu C, Peng H, Johnson PA, Leclerc M, Cao Y, Ulanski J, Li Y, Zou Y. Single-junction organic solar cell with over 15% efficiency using fused-ring acceptor with electron-deficient core. Joule 2019;3:1140–51.
[6] Yuan J, Zhang Y, Zhou L, Zhang C, Zhang C, Lau T-K, Zhang G, Lu X, Yip H-L, So SK, Beaupre S, Mainville M, Johnson PA, Leclerc M, Chen H, Peng H, Li Y, Zou Y. Fused benzothiadiazole: a building block for n-type organic acceptor to achieve high-performance organic solar cells. Adv Mater 2018;31:1807577.
[7] Liang Y, Xu Z, Xia J, Tsai S-T, Wu Y, Li G, Ray C, Yu L. For the bright future-bulk heterojunction polymer solar cells with power conversion efficiency of 7.4%. Adv Mater 2010;22:E135–8.
[8] Jeon SJ, Yu JE, Han YW, Suh IS, Moon DK. Structural optimization in the same polymer backbones for efficient polymer solar cells: relationship between steric hindrance and molecular weight. J Ind Eng Chem 2019;71:137–49.
[9] Lee TH, Kim DH, Lee EJ, Moon DK. Significant impact of monomer curvatures for polymer curved shape composition on backbone orientation and solar cell performances. J Ind Eng Chem 2018;65:195–204.
[10] Kim DG, Jin HC, Maduwu RD, Salma SA, Moon DK, Kim JH. Synthesis of new conjugated small-molecule-dyes based on 2-(2-methyl-4H-chromen-4-ylidene) malononitrile as the electron-withdrawing group and their application in photovoltaic devices. Dyes Pigments 2019;163:660–6.
[11] Handoko SL, Jin HC, Whang DR, Putri SK, Kim JH, Chang DW. Synthesis of quinoxaline-based polymers with multiple electron-withdrawing groups for polymer solar cells. J Ind Eng Chem 2019;73:192–7.
[12] Sylvianti N, Kim YH, Kim DG, Maduwu RD, Jin HC, Moon DK, Kim JH. Synthesis of conjugated materials based on benzodithiophene - benzothiadazole and their application of organic solar cells. Macromol Res 2018;26:552–6.
[13] Putri SK, Jin HC, Whang DR, Kim JH, Chang DW. Enhanced open-circuit voltages of trifluoromethylated quinoxaline-based polymer solar cells. Org Electron 2019;65:363–9.
[14] Zhao W, Qian D, Zhang S, Li S, Inganäs O, Gao F, Hou J. Fullerene-free polymer solar cells with over 11% efficiency and excellent thermal stability. Adv Mater 2016;28:4734–9.
[15] Nam SJ, Jeon SJ, Han YW, Moon DK. Effect of non-covalent interactions on molecular stacking and photovoltaic properties in organic photovoltaics. J Ind Eng Chem 2018;63:191–200.
[16] Zhao W, Li S, Yao H, Zhang S, Zhang Y, Yang B, Hou J. Molecular optimization enables over 13% efficiency in organic solar cells. J Am Chem Soc 2017;139:7148–51.
[17] Heo H, Kim H, Nam G, Lee D, Lee Y. Multi-donor random terpolymers based on benzodithiophene and dithienosilole segments with different monomer compositions for high-performance polymer solar cells. Macromol Res 2018;26:238–45.
[18] Jo MY, Ha YE, Kim JH. Polyviologen derivatives as an interfacial layer in polymer solar cells. Sol Energy Mater Sol Cells 2012;107:1–8.
[19] Jin X, Wang Y, Cheng X, Zhou H, Hu L, Zhou Y, Chen L, Chen Y. Fluorine-induced self-doping and spatial conformation in alcohol-soluble interlayers for highly-efficient polymer solar cells. J Mater Chem A 2018;6:423–33.
[20] Roh SH, Kim JK. Hexagonal array patterned PMMA buffer layer for efficient hole transport and tailored interfacial properties of FTO-based organic solar cells. Macromol Res 2018;26:1173–8.
[21] Liu H, Huang L, Cheng X, Hu A, Xu H, Chen L, Chen Y. N-type self-doping of fluorinate conjugated polyelectrolytes for polymer solar cells: modulation of dipole, morphology, and conductivity. ACS Appl Mater Interfaces 2017;9:1145–53.
[22] Do TT, Hong HS, Ha YE, Park J, Kang Y-C, Kim JH. Effect of polyelectrolyte electron collection layer counteranion on the properties of polymer solar cells. ACS Appl Mater Interfaces 2015;7:3335–41.
[23] Lim GE, Ha YE, Jo MY, Park J, Kang Y-C, Kim JH. Nonconjugated anionic polyelectrolyte as an interfacial layer for the organic optoelectronic devices. ACS Appl Mater Interfaces 2013;5:6508–13.
[24] Li Y, Liu X, Li X, Zhang W, Xing F, Fang J. Electrolytes as cathode interlayers in inverted organic solar cells: influence of the cations on bias-dependent performance. ACS Appl Mater Interfaces 2017;9:8426–31.
[25] Li Z, Chen Q, Liu Y, Ding L, Zhang K, Zhu K, Yuan L, Dong B, Zhou Y, Song B. A nonconjugated zwitterionic polymer: cathode interfacial layer comparable with PFN for narrow-bandgap polymer solar cells. Macromol Rapid Commun 2018;39:1700828.
[26] Gupta M, Yan D, Xu J, Yao J, Zhan C. Tetraphenylphosphonium bromide as a cathode buffer layer material for highly efficient polymer solar cells. ACS Appl Mater Interfaces 2018;10:5569–76.
[27] Shao S, Zheng K, Pullerits T, Zhang F. Enhanced performance of inverted polymer solar cells by using poly(ethylene oxide)-modified ZnO as an electron transport layer. ACS Appl Mater Interfaces 2013;5:380–5.
[28] Kim YH, Kim DG, Kim JH. ZnO-free inverted polymer solar cells based on new viologen derivative as a cathode buffer layer. Appl. Chem. Eng. 2016;27:512–5.
[29] Do TT, Hong HS, Ha YE, Park C-Y, Kim JH. Investigation of the property change of polymer solar cells by changing counter anions in polyviologen as a cathode buffer layer. Macromol Res 2015;23:177–82.
[30] Wu Z, Sun C, Dong S, Jiang X-F, Wu S, Wu H, Yip H-L, Huang F, Cao Y. N-type water/alcohol-soluble naphthalene diimide-based conjugated polymers for high-performance polymer solar cells. J Am Chem Soc 2016;138:2004–13.
[31] Xu G, Gao L, Xu H, Huang L, Xie Y, Cheng X, Li Y, Chen L, Chen Y. N-type conjugated electrolytes cathode interlayer with thickness-insensitivity for highly efficient organic solar cells. J Mater Chem A 2017;5:13807–16.
[32] Kim YH, Sylvianti N, Marsya MA, Park J, Kang Y-C, Moon DK, Kim JH. A simple approach to fabricate an efficient inverted polymer solar cell with a novel small

molecular electrolyte as the cathode buffer layer. ACS Appl Mater Interfaces 2016; 8:32992–7.
[33] Kim YH, Sylvianti N, Marsya MA, Moon DK, Kim JH. Properties of inverted polymer solar cells based on novel small molecular electrolytes as the cathode buffer layer. Org. Electron. Physics, Mater. Appl. 2016;39:163–7.
[34] Guo X, Zhang Y, Liu X, Braun S, Wang Z, Li B, Li Y, Duan C, Fahlman M, Tang J, Fang J, Bao Q. Novel small-molecule zwitterionic electrolyte with ultralow work function as cathode modifier for inverted polymer solar cells. Org Electron 2018; 59:15–20.
[35] Kim DG, Kim YH, Maduwu RD, Jin HC, Moon DK, Kim JH. Organic electrolyte hybridized ZnO as the electron transport layer for inverted polymer solar cells. J Ind Eng Chem 2018;65:175–9.
[36] Kim YH, Kim DG, Maduwu RD, Jin HC, Moon DK, Kim JH. Organic electrolytes doped ZnO layer as the electron transport layer for bulk heterojunction polymer solar cells. Sol. RRL. 2018;2:1800086.
[37] Ouyang X, Peng R, Ai L, Zhnag X, Ge Z. Efficient polymer solar cells employing a non-conjugated small-molecule electrolyte. Nat Photonics 2015;9:520–4.
[38] Liu Z, Ouyang X, Peng R, Bai Y, Mi D, Jiang W, Facchetti A, Ge Z. J Mater Chem A 2016;4:2530–6.
[39] Nho S, Baek G, Park S, Lee BR, Cha MJ, Lim DC, Seo JH, Oh S-H, Song MH, Cho S. Highly efficient inverted bulk-heterojunction solar cells with a gradiently-doped ZnO layer. Energy Environ Sci 2016;9:240–6.
[40] Han JP, Lee EJ, Han YW, Lee TH, Moon DK. Enhancement in performance of polymer solar cells by introducing solution-processed dipole interlayer. J Ind Eng Chem 2016;36:44–8.
[41] Chang S-Y, Lin Y-C, Sun P, Hsieh Y-T, Meng L, Bae S-H, Su Y-W, Huang W, Zhu C, Li G, Wei K-H, Yang Y. High-efficiency organic tandem solar cells with effective transition metal chelates interconnecting layer. Sol. RRL. 2017;1:1700139.
[42] Soultati A, Fakharuddin A, Polydorou E, Drivas C, Kaltzoglou A, Haider MI, Kournoutas F, Fakis M, Palilis LC, Kennou S, Davazoglou D, Falaras P, Argitis P, Gardelis S, Kordatos A, Chroneos A, Schmidt-Mende L, Vasilopoulou M. Lithium doping of ZnO for high efficiency and stability fullerene and non-fullerene organic solar cells. ACS Appl Energy Mater 2019;2:1663–75.
[43] Yip H-L, Hau SK, Baek NS, Ma H, Jen AK-Y. Polymer solar cells that use self-assembled-monolayer-modified ZnO/metals as cathodes. Adv Mater 2008;20: 2376–82.
[44] Upama MB, Elumalai NK, Mahmud MA, Wright M, Wang D, Xu C, Haque F, Chan KH, Uddin A. Interfacial engineering of electron transport layer using caesium iodide for efficient and stable organic solar cells. Appl Surf Sci 2017;416: 834–44.
[45] Li H, Zhang R, Qu Y, Zhang J. The bi-direction tuning of work function by authigenic buffer layer in all polymer solar cells. Appl Surf Sci 2018;447:63–71.
[46] Lee D-Y, Cho S-P, Na S-I, Kim S-S. ITO-free polymer solar cells with vanadium oxide hole transport layer. J Ind Eng Chem 2017;45:1–4.
[47] Jung SE, Lee EJ, Moon DK, Haw JR. Surface modification of line-patterned electron transfer layer for enhancing the performance of organic solar cells. J Ind Eng Chem 2017;52:147–52.
[48] Mortimer RJ. Five color electrochromicity using prussian blue and nafion/methyl viologen layered films. J Electrochem Soc 1991;138:633–4.
[49] Ku GM, Lee E, Kang B, Lee JH, Cho K, Lee WH. Relationship between the dipole moment of self-assembled monolayers incorporated in graphene transistors and device electrical stabilities. RSC Adv 2017;7:27100–4.
[50] Jin H, O'Hare B, Dong J, Arzhantsev S, Baker GA, Wishart JF, Benesi AJ, Maroncelli M. Physical properties of ionic liquids consisting of the 1-butyl-3-methylimidazolium cation with various anions and the bis (trifluoromethylsulfonyl)imide anion with various cations. J Phys Chem B 2008; 112:81–92.
[51] Cavalcante ADO, Ribeiro MCC, Skaf MS. Polarizability effects on the structure and dynamics of ionic liquids. J Chem Phys 2014;140:144108.
[52] Studzińska S, Molíková M, Kosobucki P, Jandera P, Buszewski B. Study of the interactions of ionic liquids in IC by QSRR. Chromatographia 2011;73:35–44.
[53] Bagui A, Iyer SSK. Increase in hole mobility in poly (3-hexylthiophene-2,5-diyl) films annealed under electric field during the solvent drying step. Org Electron 2014;15(7):1387–95.
[54] Parker ID. Carrier tunneling and device characteristics in polymer light-emitting diodes. J Appl Phys 1994;75:1656.